SERBIAN JOURNAL OF ELECTRICAL ENGINEERING
Vol. 16, No. 1, February 2019, 105-121

UDC: 621.373+621.391]:004.94 **DOI: https://doi.org/10.2298/SJEE1901105N**

Analysis and Design of LCS Resonant Cell Based Enhanced Zero-Voltage Transition DC-DC Boosting Converter

Anandh Nagarajan[1], Sekaran Julius Fusic[2]

Abstract: An enhanced zero-voltage transition boosting converter (EZVTBC) is introduced here which belongs to higher-order family. It exhibits lower source current and load voltage ripples and also it maintains better voltage gain with respect to traditional step-up converter. The zero-voltage transition is attained with an aid of a LCS resonant cell integrating $L_r - C_r$ resonance tank network along with an extra switch. LCS resonant cell is the modified version of conventional ZVT switch cell and the salient feature of this cell is to eliminate peak current stress and conduction losses of main switch as this remains a predominant problem in hard-switched boost converter and it also improves efficiency. Initially, time domain expressions of EZVTBC are derived using Kirchhoff's laws for different operational stages to predict the resonant transition phenomenon. The simulation is progressed in PSIM software in order to verify its soft-switching performance on a 12 – 24 V, 30 W converter and also dynamic performance of the converter has been studied with line and load variations. It is found that for rated load conditions, efficiency of the soft-switched converter is improved 5 to 10% approximately and resulted in 97%. Moreover the peak current stress and conduction losses were eliminated.

Keywords: Enhanced ZVT Boosting Converter, LCS resonant cell, Soft-Switching, Zero-Voltage Transition, Peak Current Stress.

1 Introduction

Boosting DC-DC converters normally used for obtaining higher output voltages fed from lower input source. The conventional boost converters exhibits many drawbacks like higher duty ratio, low efficiency and high switching losses etc. To rectify these problems higher-order PWM based boosting converters are employed. These higher-order converters provides good efficiency and voltage gain [3]. Higher-order converters like fourth-order

[1]Department of Electrical and Electronics Engineering, Manipal Institute of Technology, Manipal Academy of Higher Education, Manipal – 576 104, Karnataka, India; E-mail: anandh.n@manipal.edu
[2]Department of Mechatronics Engineering, Thiagarajar College of Engineering, Madurai – 625 015, Tamil Nadu, India; E-mail: sjf@tce.edu

converters possess better voltage gain, reduced source current and load voltage ripples compare to second-order converters. They also needed for meeting various source and load requirements [7].

Improvement of efficiency in converters is done through soft-switching methods very efficiently. There are two basic schemes namely zero-voltage switching and zero-current switching. These two schemes primarily concentrates on improving the efficiency only, but there are few drawbacks in these techniques, they are (i) increased conduction losses (ii) increased stresses of current and voltage. These limitations be able to resolve by soft-transition methods namely zero-voltage transition and zero-current transition. The ZVS scheme based quasi-resonant converters decreases the switching losses but raises the current and voltage stresses leading to increased conduction losses, thus ZVT scheme is very essential to reduce the voltage and current stresses [1 – 2]. To remove the switch and transition losses occurring in hard-switched converters, several procedures of soft-switching are discussed [4 – 5]. The integration of ancillary network reduces the losses and improves the voltage gain [6].

An improved ZVT soft-switching boost converter minimizes the switch turn-off losses of additional switch by employing a supplementary network and also a method for reducing the voltage spike were addressed [8]. An inductor feedback method of modified zero-voltage transition boost converter was discussed, wherein an inductor coupled with zener diode is used to minimize the conduction loss of ancillary switch [9]. Analysis of fifth-order zero-voltage transition boost converter was done such that it offers high voltage gain and reduced switching losses with an aid of $L_r - C_r$ resonating circuit [10].

A snubber cell based pulse width modulation converter was established to rise the power density, efficiency and also to reduce the EMI noise [11, 13]. A PWM based phase shift full bridge converter was introduced with outer snubber capacitors parallel linked with IGBT's to reduce turn-off losses and improve efficiency [12]. By considering the diode reverse-recovery effect, analysis of zero-voltage transition bidirectional converter was done in order to improve its soft-switching range [14]. A new magnetically coupled bidirectional non-isolated dc-dc converters are proposed consisting of a simple additional circuit in order to obtain soft-transition operation in both power flow directions [15, 16, 19, 21].

An improved Z – source circuit based high step-up dc-dc converter was introduced, wherein conduction losses and switch current stress are reduced by using only one magnetic core in which all other inductors are coupled [17]. A new DC-DC converter was proposed for PV based renewable energy conversion systems with solar cell as an input. This converter is basically a boost converter with voltage-doubler configuration in order to attain high step-up conversion

ratio [18]. A soft-switched interleaved boost converter was suggested which reduces conduction losses and removes the reverse-recovery issue by employing soft-switching cell [20]. A new soft-switched dc-dc converter which has less voltage and current stress with ZVS turn-on feature for all active switches and applicable for high source voltage and load current applications was explored [22 – 23].

Since there are no much work done on soft-switching higher-order converters, especially fourth and fifth-order converters by using ZVT technique, this paper focussed on implementation of enhanced ZVT technique on a fourth-order converter. Therefore, the main objective here is to visualize resonant transition phenomenon for all devices employed in the converter by using LCS resonant cell. The LCS resonant cell is the improved version of conventional ZVT switch cell eliminates main switch high current stress and conduction losses, moreover it improves the efficiency.

This paper is organized in such a way that it describes about the converter circuit in Section 2, Section 3 projects the operating principle and time domain analysis of EZVTBC, gating sequence of switches and power stage components design parameters are given in Section 4 followed by formulation of control-to-output voltage transfer function in Section 5. Lastly results and conclusion were deliberated in Sections 6 and 7.

2 Circuit Description of the Converter

An improved soft-switching auxiliary network is introduced into the conventional hard-switched boost converter. The additional circuit comprises of an ancillary switch (S_A), an energy transferring capacitor (C_r), an energy transferring inductor (L_r) called as LCS resonant cell is shown in Fig. 1, an additional inductor in series with main switch (L_M) helps in achieving better soft-switching. The equivalent network of suggested converter (EZVTBC) is depicted in the Fig. 2. Here, the converter main and ancillary switch are operating under ZVT conditions. The switches S_M and S_A are operating in synchronized switching pattern to achieve the soft-switching conditions and improve the efficiency from lighter load to full load. The resonance is taking place between the energy transferring capacitor (C_r) and energy transferring inductor (L_r) and also for shorter interval resonating capacitor exchanges energy with the parallel combination of L_r and L_M. The selection of C_r, L_r and L_M is significant because those are the key elements in achieving the proper ZVT operations. This converter undergoes six different stages of operation in a switching cycle. The main converter circuit is replaced with its equivalent circuit by considering few assumptions in order to make the time domain analysis simpler. At source side, existence of huge inductor (L_1) in series with voltage source is substituted by a constant current source (I_g). At load side,

existence of huge capacitor (C_0) in parallel with load is substituted by a constant voltage source (V_0). Assuming all the switching devices and energy storing elements are ideal.

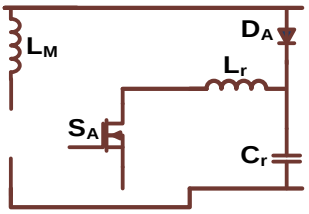

Fig. 1 – *LCS resonant cell.*

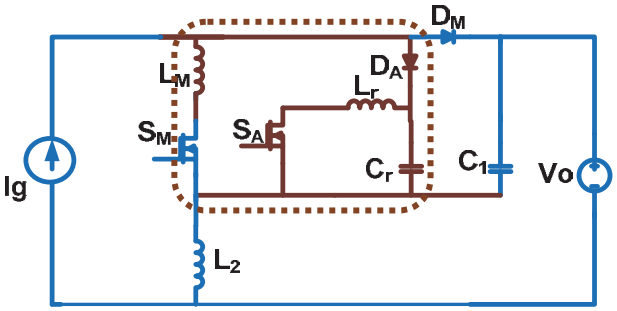

Fig. 2 – *Main equivalent circuit of EZVTBC.*

3 Operating Principle and Time Domain Analysis of EZVTBC

Stage I: ($t_0 < t < t_1$)

Prior to this stage, the circuit was in freewheeling mode with D_M alone conducting. In this stage of operation before turning on main switch, turning on the auxiliary switch reduces main switch voltage to zero.

Initial Conditions:

$$v_{C_r}(0) = V_0, \quad i_{L_r}(0) = 0, \quad i_{D_A}(0) = 0$$

By applying KVL along different meshes in the circuit, we get,

$$v_{C_1} = v_{C_r} \tag{1}$$

$$v_{L_r} = v_{C_r}. \tag{2}$$

By applying KCL at various nodes in the circuit, we get,

$$I_g = i_{D_A} + i_{D_M}, \tag{3}$$

$$i_{D_A} + i_{C_r} = i_{L_r}, \tag{4}$$

$$i_{D_M} = i_{C_1} + \frac{V_0}{R}. \tag{5}$$

By doing further mathematical simplification, resonant capacitor voltage can be obtained in *s*-domain and it can be transformed into time domain equation at the end of this stage.

$$\left(v_{C_r}(s)\right) = \frac{sV_0}{\left(s^2 + \frac{1}{L_r\{(C_1 - C_r)\}}\right)}, \tag{6}$$

$$v_{C_r}\left(t^1\right) = V_0 \cos\left[\omega_{r1}(t - t_0)\right], \tag{7}$$

where

$$\omega_{r1} = \sqrt{\frac{1}{L_r\left[(C_1 - C_r)\right]}}, \tag{8}$$

$$i_{D_A}\left(t^1\right) = \frac{2V_0}{Z_r}\sin\left[\omega_{r1}(t - t_0)\right], \tag{9}$$

where

$$Z_r = \sqrt{\frac{L_r}{C_r}}. \tag{10}$$

Since

$$I_g = i_{D_A} + i_{D_M}, \tag{11}$$

$$i_{D_M}\left(t^1\right) = I_g - \frac{2V_0}{Z_r}\sin\left[\omega_{r1}(t - t_0)\right]. \tag{12}$$

At $t = t_1$, this stage completes, making the current through main diode to zero.

$$t_1 = \frac{1}{\omega_{r1}}\sin^{-1}\left(\frac{I_g Z_r}{2V_0}\right). \tag{13}$$

Stage II: ($t_1 < t < t_2$)

Second stage deals with the ancillary switch and diode in switched on condition. As this stage concludes, the main switch voltage goes to zero and favourable ZVS turn-on condition of main switch will prevail.
Initial Conditions:

$$v_{C_r}(0) = V_0 \cos\left[\omega_{r1}(t_1 - t_0)\right], \quad i_{L_r}(0) = \frac{V_0}{Z_r}\sin\left[\omega_{r1}(t_1 - t_0)\right], \quad i_{D_A}(0) = I_g .$$

By applying KVL along mesh, we get,

$$v_{L_r} = -v_{C_r} . \tag{14}$$

By applying KCL at node, we get,

$$i_{L_r} = i_{D_A} + i_{C_r} . \tag{15}$$

Time domain equation can be obtained by simplifying resonant capacitor voltage expression and also resonant inductor current expression can be derived.

At $t = t_2, v_{C_r}(t_2) = 0$

$$0 = V_0 \cos\left[\omega_{r1}(t_1 - t_0)\right]\cos\left[\omega_r(t - t_1)\right] - V_0 \sin\left[\omega_{r1}(t_1 - t_0)\right]\sin\left[\omega_r(t - t_1)\right], \tag{16}$$

$$t_2 = t_1 + \left(\frac{1}{\omega_{r1}}\right)\tan^{-1}\left[\cot\left\{\omega_r\left(t_1 - t_0\right)\right\}\right], \tag{17}$$

$$i_{L_r}(t^1) = I_g - \frac{V_0}{Z_r}\left[\sin\left[\left\{\omega_r(t - t_1)\right\} - \left\{\omega_{r1}(t_1 - t_0)\right\}\right]\right]. \tag{18}$$

Stage III: ($t_2 < t < t_3$)

In this stage, the main switch body-diode turns on along with auxiliary switch and diode. Wherein the diode is already in switched on condition. During this stage resonant capacitor starts charging.

Initial Conditions:

$$v_{C_r}(0) = 0, \quad i_{L_r}(0) = I_g - \frac{V_0}{Z_r}\left[\sin\left\{\omega_r(t_2 - t_1) - \omega_{r1}(t_1 - t_0)\right\}\right], \quad i_{D_A}(0) = I_g .$$

By applying KVL along mesh, we get

$$v_{L_r} = v_{C_r} , \tag{19}$$

$$i_{L_r}(t^1) = \frac{I_g Z_r}{L_r}\left[(t - t_2) + \frac{e^{-\omega_r(t - t_2)}}{\omega_r}\right] - I_g + \frac{V_0}{Z_r}\left[\sin\left\{\omega_r(t_2 - t_1) - \omega_{r1}(t_1 - t_0)\right\}\right], \tag{20}$$

By applying KCL at node, we get

$$i_{L_r} = i_{D_A} - i_{C_r} . \tag{21}$$

Simplification of resonant capacitor voltage expression leads to time domain equation and current expression of L_M can be derived.

$$\left(v_{C_r}(s)\right) = I_g Z_r\left(\frac{1}{s} - \frac{1}{(s + \omega_r{}^2)}\right), \tag{22}$$

$$\left(v_{C_r}\left(t-t_2\right)\right)=I_g Z_r\left(1-e^{-\omega_r(t-t_2)}\right), \tag{23}$$

$$i_{L_M}(t^1)=I_g-\frac{2V_0}{Z_r}\left[\sin\left\{\omega_r(t_2-t_1)-\omega_{r1}(t_1-t_0)\right\}\right]. \tag{24}$$

Stage IV: ($t_3 < t < t_4$)

In this operational mode, only main switch is in on condition and resonating capacitor (C_r) charges to its full value before this stage and also L_M charges linearly through a steady source current I_g. Here, current will be flowing through main inductor, main switch and L_2.

Stage V: ($t_4 < t < t_5$)

During this operation, turning off of main switch in hard-switching condition leads to the turning on of auxiliary diode. In this stage, current will be flowing through ancillary diode, resonant capacitor and L_2.

Stage VI: ($t_5 < t < t_6$)

This stage is the resemblance of conventional boost converter, by making the main diode on, this operational stage gets completed.

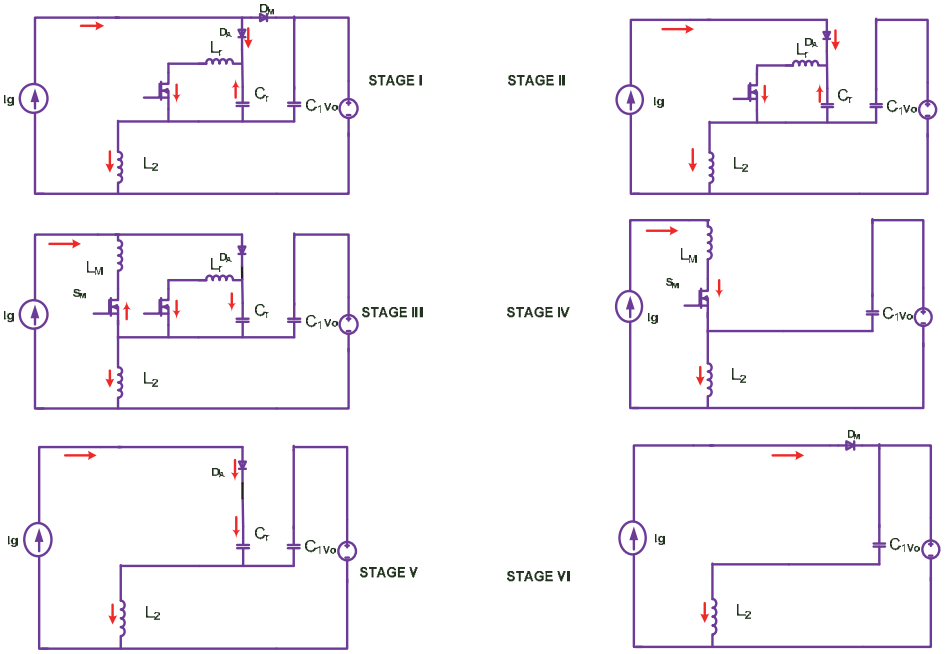

Fig. 3 – *Topological variations.*

There are few factors that destroys the resonant switching nature of the devices they are: (i) inappropriate choice of passive resonant components (ii) inaccurate gate signal time interval for ancillary switch and (iii) loss of synchronism between gate signals of both switches. Figs. 3 and 4 illustrate the structural variations and steady-state waveforms of EZVTBC. From the Fig. 3, the current flowing directions and switching devices conditions can be realized with six different equivalent networks. From Fig. 4, the nature of voltage and current waveforms of all the devices for six different operational stages and resonance occurring transition region of enhanced zero-voltage transition LCS resonant cell based boosting converter can be observed.

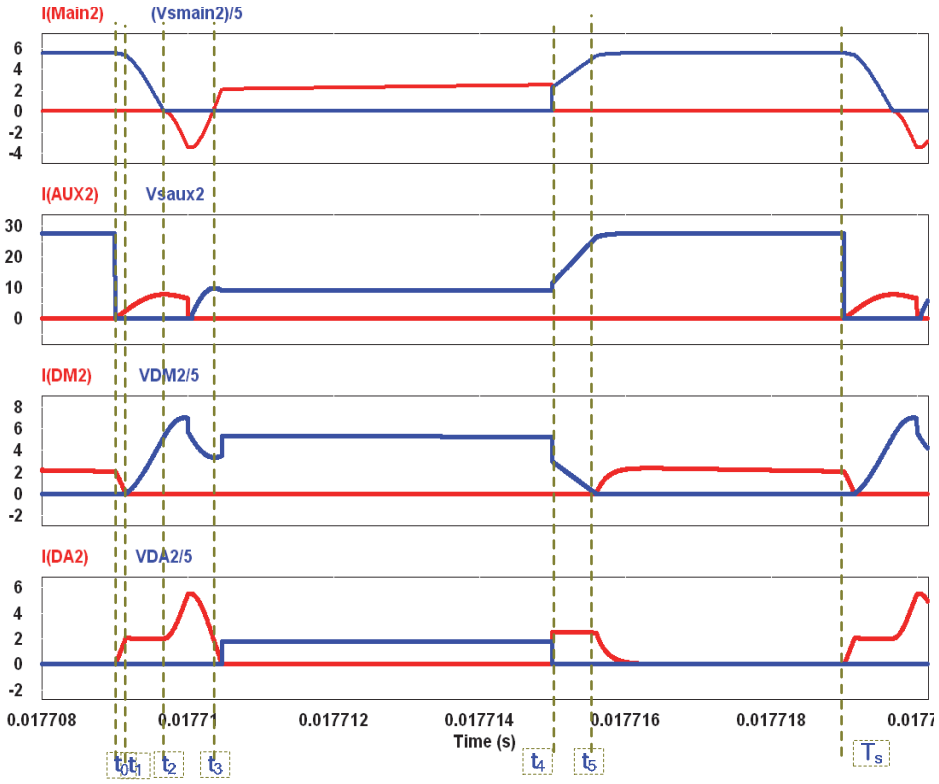

Fig. 4 – *Steady-state waveforms.*

4 Gating Sequence of Switches and Power Stage Components Design

The enhanced scheme for implementation of ZVT in the converter has the following merits, (i) main switch gating signal increasing point should be matched with ancillary switch gating signal decreasing point called as switch

synchronization points and it is simpler to implement (ii) even after the main switch is turned on, the additional switch gate pulse is to be continued for some extended time, so that soft-switching can be achieved and it is defined as time delay between the start of gate pulse for main switch and the instant of withdrawing gate pulse to the auxiliary switch. Fig. 5 depicts the gate signal waveforms for both main and additional switch.

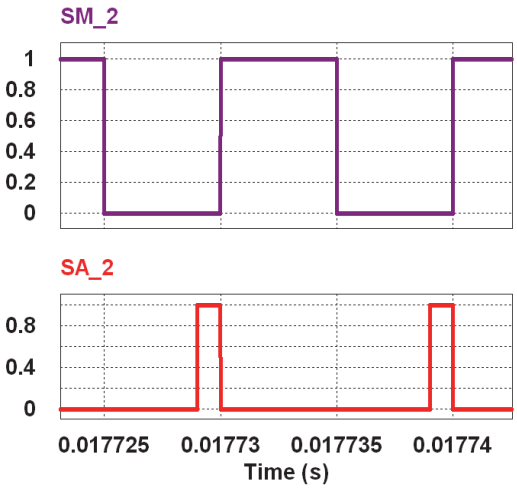

Fig. 5 – *Simulated waveforms of gating sequence of switches.*

The design parameters of the converter is given below in **Table 1**.

Table 1
Design values of power stage components.

Parameters	Design values
Power output (P_o)	30 W
Output voltage (V_o)	24 V
Switching frequency (f_s)	100 kHz
Source inductor 1 (L_1)	150 µH
Source inductor 2 (L_2)	50 µH
Load capacitor 1 (C_0)	100 µF
Load capacitor 2 (C_1)	100 µF
Resonant inductor (L_r)	0.6 µH
Resonant capacitor (C_r)	170 nF

5 Formulation of Control-to-Output Voltage Transfer Function

This higher-order converter undergoes various topological changes in one switching cycle and obtaining the transfer function of the system using state space approach is really a challenging task. Therefore by utilising system identification tool in MATLAB [25] and by Perturb and Observe method the system transfer function is achieved for various operational stages with best fit of confident interval (above 85%).

Among the two schemes of control, the effective and best control strategy is voltage-mode control because of null stability problems and switching response time is equal to cascaded control. In this work, a digitally based voltage-mode controller is utilised for achieving dynamic response of the converter.

After obtaining the plant transfer function, the compensator transfer function can be obtained which involves in achieving a desirable closed-loop performance of the system. Design of digital compensator can be achieved similarly with respect to design of traditional controller and there are two usual schemes used in these design stages namely: (i) digital re-design, (ii) digital direct design. The plant transfer function $G_p(z)$ for ZVT operation has been obtained with the help of system identification approach. Output Error (OE) method has been adapted and transfer function obtained for a best fit of 88.66% is

$$\frac{\hat{v}_o(z)}{\hat{d}(z)} = \frac{-0.04294z^3 + 0.1278z^2 - 0.1233z + 0.03841}{z^4 - 3.156z^3 + 3.513z^2 - 1.556z + 0.1997}. \tag{25}$$

The voltage-mode controller has been designed considering the above transfer function of open loop system is,

$$G_c(z) = 0.77605 \cdot \frac{(z - 0.988)(z - 0.9998)}{(z - 1)(z - 0.983)}. \tag{26}$$

Utilising the transfer function of plant $G_p(z)$ and transfer function of compensator $G_c(z)$, the GM, PM and Band Width values for the designed controller are attained from the Bode and Root locus plots of the converter loop gain with controller and the matching figures are depicted in Figs. 6 and 7.

From the above root locus plot characteristics, it can be witnessed that the GM is 15.1 dB, PM is 52º and the gain crossover frequency is 884 Hz, which are all under stability limitations for the controller. The Bode plots of the Converter ($G_p(z)$), Controller ($G_c(z)$) and Loop gain ($T_L(z)$) are depicted in Fig. 8.

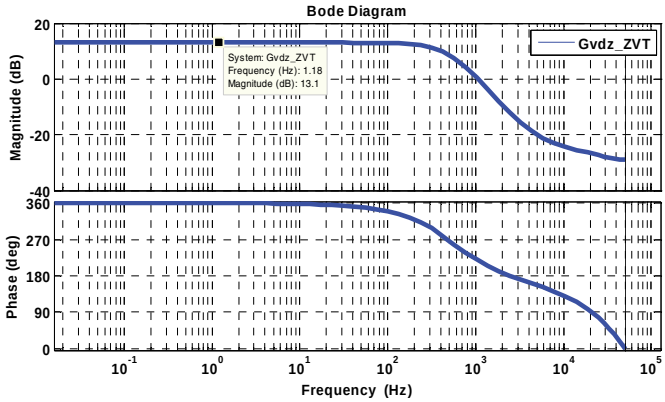

Fig. 6 – *Frequency response characteristics of EZVTBC.*

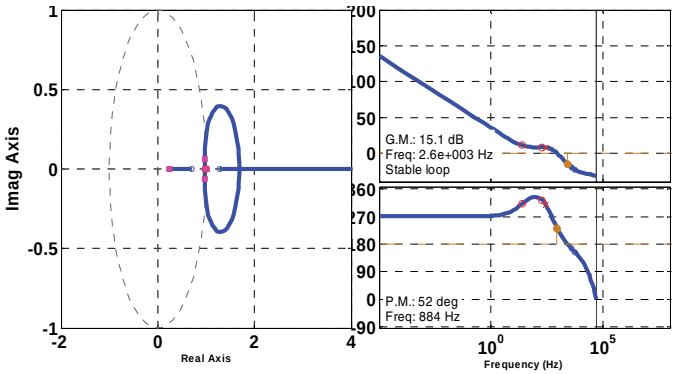

Fig. 7 – *Root locus plot of EZVTBC.*

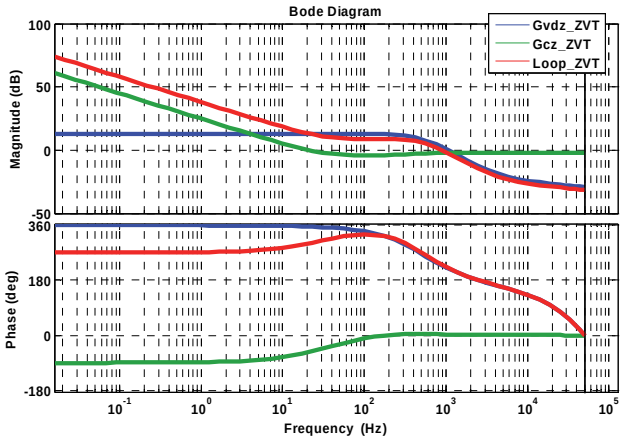

Fig. 8 – *Bode plots of EZVTBC converter (blue), compensator (green) and Loop gain (red) (GM* = 15.1 dB, *PM* = 52, f_c = 884 Hz*).*

6 Simulation Results

The main switch peak current stress during turn on transition will be reduced by incorporating the improved version of soft-switching LCS cell under consideration into the EZVTBC while achieving ZVS turn-ON of the main switch. Fig. 9 depicts the elimination of main switch peak current stress. Fig. 10 depicts the status of peak current stress in conventional ZVT cell converter and enhanced ZVT LCS cell converter. Fig. 11 depicts main switch voltage and current simulated waveforms of conventional ZVT converter and EZVTBC.

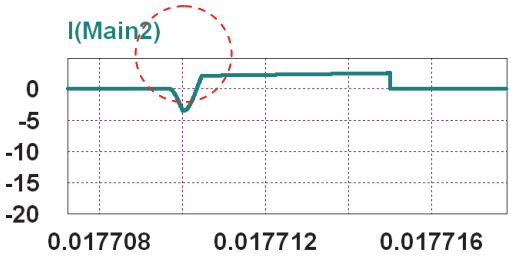

Fig. 9 – *Elimination of main switch current stress.*

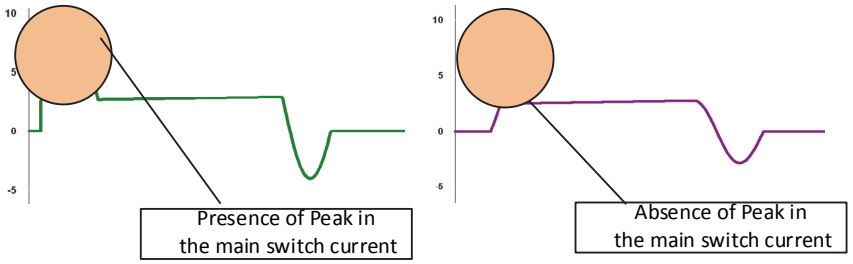

Fig. 10 – *Peak current stress in conventional ZVT cell converter and enhanced ZVT LCS cell converter.*

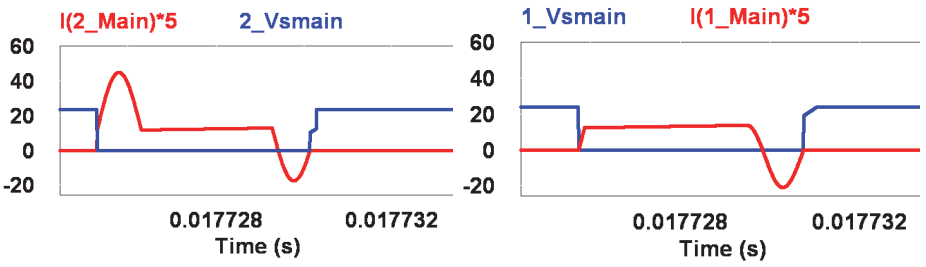

(a) (b)

Fig. 11 – *Main switch voltage and current simulated waveforms of conventional ZVT converter and EZVTBC.*

From Figs. 12 – 15 it can be concluded that along with main and auxiliary switches the LCS resonant cell is also capable of providing resonance conditions for main and ancillary diodes.Where as in conventional ZVT network, it can be seen that it is providing resonance conditions only for main switch and it is not addressing the hard-switching problem of other switching devices. The time delay between the turning OFF of auxiliary switch and turning ON of main switch does a significant job in case of conventional ZVT switch cell based soft-switching converter, where as the enhanced ZVT LCS resonant cell based soft-switching converter can achieve the soft-switching without any delay.

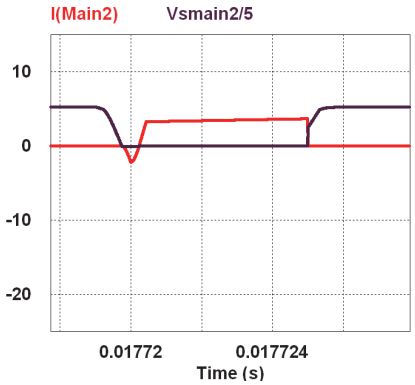

Fig. 12 – *Main switch current and voltage.*

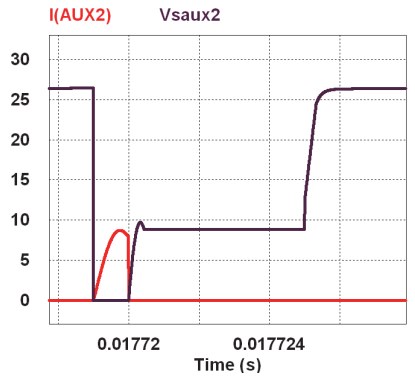

Fig. 13 – *Auxiliary switch current and voltage.*

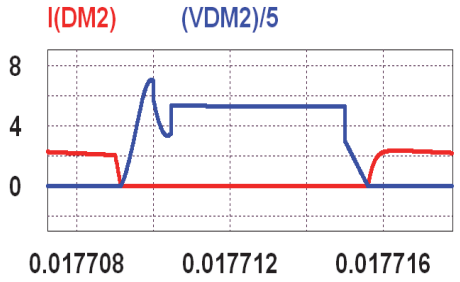

Fig. 14 – *Main diode current and voltage.*

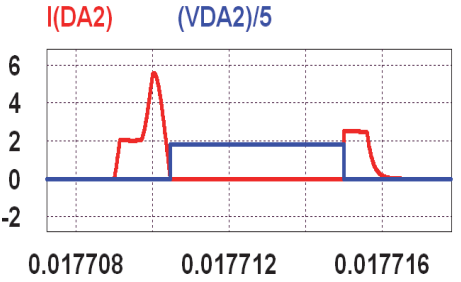

Fig. 15 – *Auxiliary diode current and voltage.*

Verification of the controller competency was carried out in PSIM simulation [24] for different line and load variations. A load variation of output resistance from 20Ω to 36Ω was created after 10 ms and load voltage of the converter was regulated within 2 ms using the controller. Sudden variation of 12 V to 15 V was created in the line voltage and the action of controller was

witnessed successfully which made the disturbances to settle down within 2 ms. The matching result is depicted in Fig. 16.

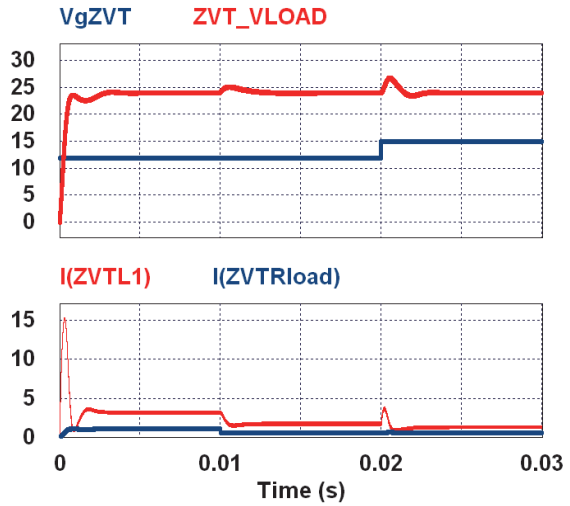

Fig. 16 – *Simulated dynamic response characteristics of EZVTBC for* (R = 20 – 36 Ω *at* t = 10 ms*;* V_g = 12 – 15 V *at* t = 20 ms*).*

Ramp disturbance of 12 V to 15 V from 20 ms to 60 ms was generated in the line voltage and the action of controller was witnessed successfully which made the disturbances to settle down within 2 ms. The matching result is depicted in Fig. 17.

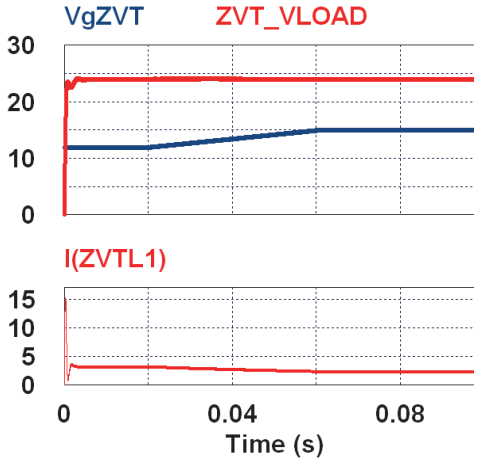

Fig. 17 – *Simulated switching performance of EZVTFBC for* (V_g = 12 – 15 V *from* 20 ms *to* 60 ms).

Theoretical efficiency and loss study for hard-switched and soft-switched converters has been done and plotted in Figs. 18 and 19, respectively. These plots depicts that at lighter loads the efficiency of the hard-switched converter is poorer and rises for increasing loads and will be maximum around nominal operating point. Where as in case of soft-switched converter its light load efficiency is also better and is almost constant throughout the vast variation in the load. The efficiency of hard-switched converter is around 87% at rated load and it is around 97% in case of soft-switched converter. The theoretical efficiencies of both hard and soft-switched converters have been plotted for the same rated load and observed that the soft-switched converter resulted in improved efficiency of about 5 to 10%.

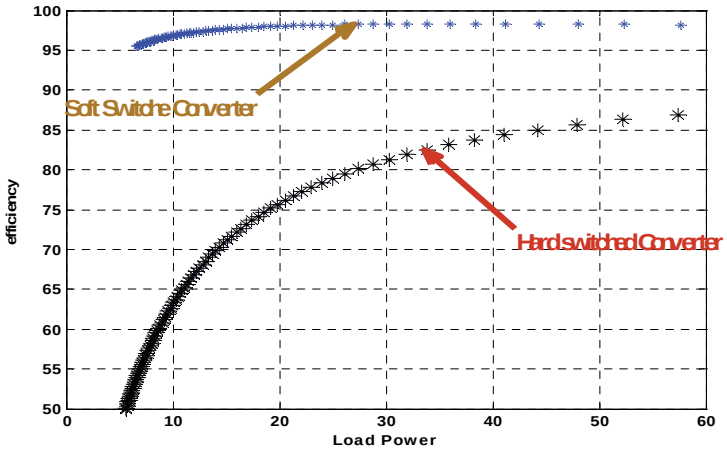

Fig. 18 – *Efficiency of hard and soft-switched converters.*

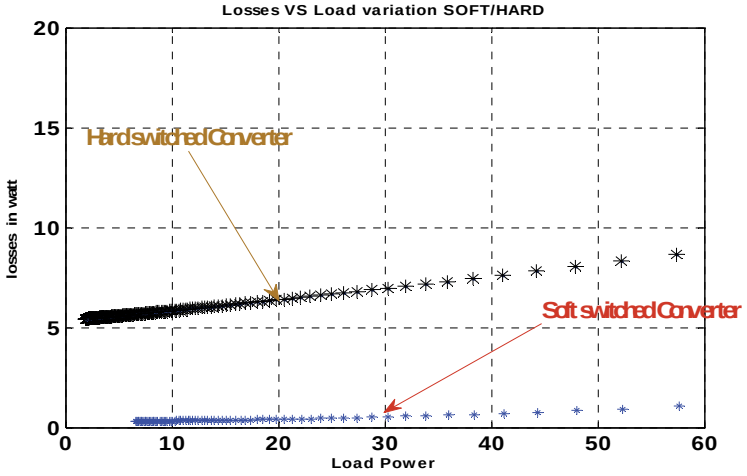

Fig. 19 – *Losses of hard & soft-switched converters.*

7 Conclusion

In this paper, the enhanced zero-voltage transition LCS resonant cell based soft-switched converter was introduced and its operational stages were explained with mathematical expressions. The enhanced zero-voltage transition boost converter is the circuit modification of traditional ZVT boost converter with extra ancillary network elements and the converter configuration is achieving ZVT for all switches and diodes, with proper gate sequence employment for both the switches. Selecting the proper resonance passive elements is of high significance so as to achieve the soft-switching operations. The ZVT condition is depending upon the duty ratio, resonance capacitance and inductance. Using the system identification tool in MATLAB the converter transfer function was derived, its Bode and Root locus plots were analysed and the controller is offering load voltage regulation for the line and load hindrances. Thus the soft-transition condition of the switches and diodes were examined and the peak current stress of main switch was removed completely, moreover the efficiency of EZVTBC has improved to 97%.

8 References

[1] G. Hua, C.- S. Leu, Y. Jiang, F. C. Y. Lee: Novel Zero-Voltage-Transition PWM Converters, IEEE Transactions on Power Electronics, Vol. 9, No. 2, March 1994, pp. 213 – 219.

[2] H.- S. Choi, B. H. Cho: Novel Zero-Current-Switching (ZCS) PWM Switch Cell Minimizing Additional Conduction Loss, IEEE Transactions on Industrial Electronics, Vol. 49, No. 1, February 2002, pp. 165 – 172.

[3] M. Veerachary: Soft-Switching Fifth-Order Boost Converter, Proceedings of the IEEE India Conference, Hyderabad, India, December 2011, pp. 1 – 4.

[4] S. Park, S. Choi: Soft-Switched CCM Boost Converters with High Voltage Gain for High-Power Applications, IEEE Transactions on Power Electronics, Vol. 25, No. 5, May 2010, pp. 1211 – 1217.

[5] J. Jiang, W. Zhang, B. Shen: Analysis and Design of a Novel ZCT-PWM Converter, The 5th International Conference on Power Electronics and Drive Systems, Singapore, November 2003, pp. 126 – 130.

[6] C.- M. Wang: Novel Zero-Voltage-Transition PWM DC–DC Converters, IEEE Transactions on Industrial Electronics, Vol. 53, No. 1, February 2006, pp. 254 – 262.

[7] M. Veerachary, A. R. Saxena: Design of Robust Digital Stabilizing Controller for Fourth-Order Boost DC-DC Converter: A Quantitative Feedback Theory Approach, IEEE Transactions on Industrial Electronics, Vol. 59, No. 2, February 2012, pp. 952 – 963.

[8] T.- W. Kim, H.- S. Kim, H.- W. Ahn: An Improved ZVT PWM Boost Converter, Proceeding of the 31st Annual Power Electronics Specialists Conference, Galway, Ireland, June 2000, pp. 615 – 619.

[9] I.- O. Lee, D.Y. Lee, B.H. Cho: Improved Zero-Voltage-Transition (ZVT) Boost Converter Using Coupled Inductor and Low-Voltage Zener Diode, Proceedings of the Power Conversion Conference, Osaka, Japan, April 2002, pp. 627 – 631.

[10] M. Veerachary, V. Verma: LCS-Cell for Zero-Voltage Transition of Fifth-Order Boost Converter, 6th International Conference on Power Systems (ICPS), New Delhi, India, March 2016, pp.1 – 6.

[11] I. Aksoy, H. Bodur, A. F. Bakan: A New ZVT-ZCT-PWM DC–DC Converter, IEEE Transactions on Power Electronics, Vol. 25, No. 8, August 2010, pp. 2093 – 2105.

[12] A. F. Bakan, N. Altintas, I. Aksoy: An Improved PSFB PWM DC–DC Converter for High-Power and Frequency Applications, IEEE Transactions on Power Electronics, Vol. 28, No. 1, January 2013, pp. 64 – 74.

[13] B. Akin: An Improved ZVT–ZCT PWM DC–DC Boost Converter with Increased Efficiency, IEEE Transactions on Power Electronics, Vol. 29, No. 4, April 2014, pp. 1919-1926.

[14] M. R. Mohammadi, H. Farzanehfard: Analysis of Diode Reverse Recovery Effect on the Improvement of Soft-Switching Range in Zero-Voltage-Transition Bidirectional Converters, IEEE Transactions on Industrial Electronics, Vol. 62, No. 3, March 2015, pp. 1471 – 1479.

[15] S. Dusmez, A. Khaligh, A. Hasanzadeh: A Zero-Voltage-Transition Bidirectional DC/DC Converter, IEEE Transactions on Industrial Electronics, Vol. 62, No. 5, May 2015, pp. 3152 – 3162.

[16] G. Chen, Y. Deng, L. Chen, Y. Hu, L. Jiang, X. He, Y. Wang: A Family of Zero-Voltage-Switching Magnetic Coupling Nonisolated Bidirectional DC–DC Converters, IEEE Transactions on Industrial Electronics, Vol. 64, No. 8, August 2017, pp. 6223 – 6233.

[17] B. Poorali, H. M. Jazi, E. Adib: Improved High Step-Up Z-Source DC–DC Converter With Single Core and ZVT Operation, IEEE Transactions on Power Electronics, Vol. 33, No. 11, November 2018, pp. 9647 – 9655.

[18] B. R. Lin, J. Y. Dong: New Zero-Voltage Switching DC–DC Converter for Renewable Energy Conversion Systems, IET Power Electronics, Vol. 5, No. 4, April 2012, pp. 393 – 400.

[19] M. R. Mohammadi, H. Farzanehfard: A New Family of Zero-Voltage-Transition Nonisolated Bidirectional Converters with Simple Auxiliary Circuit, IEEE Transactions on Industrial Electronics, Vol. 63, No. 3, March 2016, pp. 1519 – 1527.

[20] J.- H. Yi, W. Choi, B.- H. Cho: Zero-Voltage-Transition Interleaved Boost Converter with an Auxiliary Coupled Inductor, IEEE Transactions on Power Electronics, Vol. 32, No. 8, August 2017, pp. 5917 – 5930.

[21] M. R. Mohammadi, H. Farzanehfard: New Family of Zero-Voltage-Transition PWM Bidirectional Converters with Coupled Inductors, IEEE Transactions on Industrial Electronics, Vol. 59, No. 2, February 2012, pp. 912 – 919.

[22] B.- R. Lin, S.- K. Chung: New Parallel ZVS Converter with Less Active Switches and Smaller Output Inductance, IEEE Transactions on Power Electronics, Vol. 29, No. 7, July 2014, pp. 3297 – 3307.

[23] N. Anandh: Double Input Soft-Transition DC-DC Converter for Photo-Voltaic Applications, International Conference on Recent Trends in Electronics Information & Communication Technology (RTEICT), Bangalore, India, May 2016, pp. 2135 – 2139.

[24] PSIM User's Guide, Powersim, Inc., Rockville, USA, 2007.

[25] MATLAB User Manual, 2005.